MATERIALS SCIENCE

Ultrastable metallic glass by room temperature aging

Yong Zhao[1,2], Baoshuang Shang[1], Bo Zhang[1,3]*, Xing Tong[1], Haibo Ke[1]*, Haiyang Bai[1,2]*, Wei-Hua Wang[1,2]

Glasses have markedly different stability around their glass transition temperature (T_g), and metallic glasses (MGs) are conventionally regarded as metastable compared to other glasses such as silicate glass or amber. Here, we show an aging experiment on a Ce-based MG around its T_g (~0.85T_g) for more than 17 years. We find that the MG with strong fragility could transform into kinetic and thermodynamic hyperstable state after the long-term room temperature aging and exhibits strong resistance against crystallization. The achieved hyperstable state is closer to the ideal glass state compared with that of other MGs and similar to that of the million-year-aged amber, which is attributed to its strong fragility and strong resistance against nucleation. It is also observed through the asymmetrical approaching experiment that the hyperaged Ce-based MG can reach equilibrium liquid state below T_g without crystallization, which supports the idea that nucleation only occurs after the completion of enthalpy relaxation.

INTRODUCTION

Metallic glasses (MGs), originating from rapid quenching process and inheriting aperiodic structure from their melts, are in a thermodynamic and kinetic metastable state with respect to their corresponding crystalline counterparts. Upon heating above or staying for a sufficient time slightly below glass transition temperature (T_g), they are prone to aging with the deterioration of various properties and even crystallize (*1*, *2*). However, different glassy materials have completely different thermodynamic and kinetic stability. For example, amber (*3*, *4*) and silicide glasses (*5*) are extremely stable that they can maintain a glassy state for billions of years, while MGs are usually metastable (*2*), e.g., the first developed Au-Si MG started to crystallize after aging for only 3 hours at room temperature (RT) and fully crystallized after 24 hours (*6*). Although tremendous researches on the thermal stability of MGs have been conducted (*7*, *8*), the maximum annealing time was restricted to hours or days; owing to that, long-term and high-temperature annealing under laboratory conditions is extremely difficult. So far, there are rarely literatures about ultralong-time annealing investigation around their T_g (for most MGs, their T_g is around hundreds of centigrade degrees) on MGs (*7*, *9*, *10*). Therefore, it is still a controversial issue whether long-term annealing slightly below T_g will eventually result in devitrification or an ultrastable state for MGs.

Ultrastable glasses with both thermodynamic and kinetic stability have been pursued by different methods (*3*, *4*, *11*), among which vapor deposition has been widely applied to synthesize ultrastable organic (*11*–*13*) or metallic (*14*, *15*) glasses. These ultrastable organic glasses were achieved by vapor deposition method under proper substrate temperature and deposition rate to allow their constituents to sufficiently rearrange and explore stable configurations (*16*), then resulting in the formation of an ultrastable state that is only 3.9% from the valley bottom of the potential energy landscape (PEL) (*13*). However, in general, ultrastable metallic film glasses formed by deposition (*14*, *15*) have only achieved temporary kinetic stability rather than the final thermodynamic stability. It is believed that annealing method, validated by a million-year-old amber (*3*, *4*), is an effective route for obtaining ultrastable MGs. Compared with organic glass, MG with metallic bonding is expected to be able to relax into a deeper basin in PEL. Prolonged aging of Zr-, Al-, and Ni-based MGs for more than 10 years at RT has been investigated, while their aging temperature at RT is much below their relatively high T_g, and these MGs aged at RT only show slight aging and almost remain their initial amorphous structure (*10*).

Ce-based MGs, with ultralow T_g close to RT, belong to the strongest glass-forming liquid among the MG family (*17*, *18*). Their relatively low T_g provides an ideal natural aging window at RT for prolonged aging experiment on MG. In this study, a typical $Ce_{70}Al_{10}Cu_{20}$ MG with a low T_g of 353 K was applied for the investigation of prolonged aging effect around its T_g (aging at RT is equivalent to aging at 0.85T_g) for 17.7 years. It is remarked that the T_g of $Ce_{70}Al_{10}Cu_{20}$ MG is taken as the limiting fictive temperature of the rejuvenated sample throughout this article. The aging process was monitored by the evolution of its specific heat and enthalpy, and its closeness to the ideal glassy state was assessed by the alteration of the fictive temperature. We show that the MG was aged into a hyperstable state that tends toward the ideal glassy state, which is similar to the long-term aging effect observed on the million-year-old amber (*3*, *4*). The mechanism of stability of the glass is discussed on the basis of the PEL and classical nucleation theory. We further study the controversial issue about the sequence of enthalpy relaxation and nucleation in the present hyperaged Ce-based MG.

RESULTS

Structural characterization

As-cast $Ce_{70}Al_{10}Cu_{20}$ MG was naturally stored under ambient condition for a period of ~17.7 years (6443 days). The RT aging is equivalent to aging at 0.85T_g for the Ce-based MG as shown in Fig. 1A and is only about aging at 0.45T_g for Zr-based MG. Obviously, the RT aging effect on Ce-based MG is much stronger than that of other MGs with higher T_g (see table S1). To our knowledge, such a long-time aging investigation close to its T_g of MG has never been reported before. The phase structure of the aged MG at RT was reexamined by x-ray diffraction (XRD). The XRD patterns for the rejuvenated and 17.7-year-aged $Ce_{70}Al_{10}Cu_{20}$ MGs are given in Fig. 1B, where both exhibit a broad diffraction peak, indicating an amorphous structure.

[1]Songshan Lake Materials Laboratory, Dongguan, Guangdong 523808, China. [2]Institute of Physics, Chinese Academy of Sciences, Beijing 100190, China. [3]School of Materials Science and Engineering, Hefei University of Technology, Hefei 230009, China.
*Corresponding author. Email: zhangbo@sslab.org.cn (B.Z.); kehaibo@sslab.org.cn (H.K.); hybai@iphy.ac.cn (H.B.)

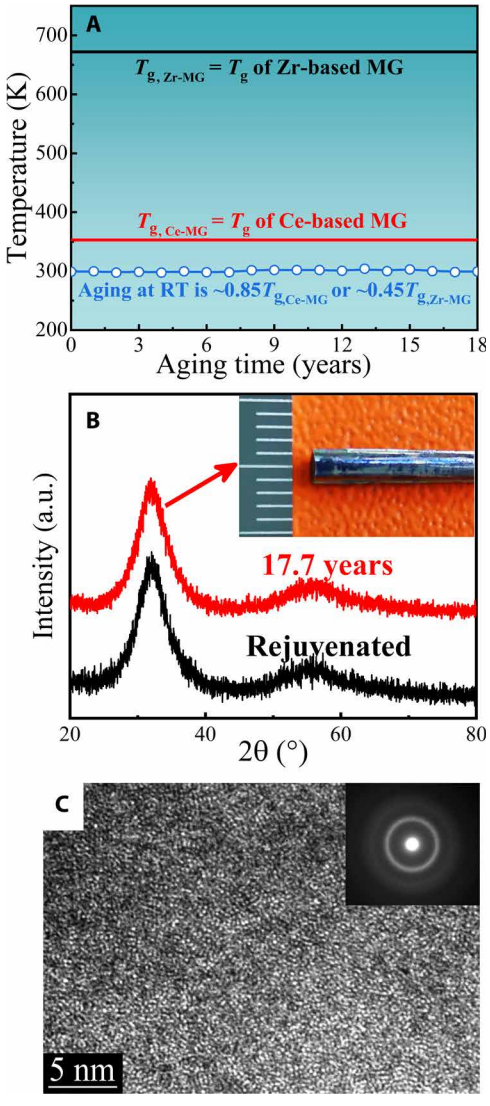

Fig. 1. Temperature profile for prolonged aging of 17.7 years around RT and the resulting structure feature of $Ce_{70}Al_{10}Cu_{20}$ MG. (**A**) The RT aging of the Ce-based MG is equivalent to aging at 0.85T_g, which is much higher than that of other MG. For example, for Zr-based MG, the RT aging is only equivalent to aging at 0.45T_g. (**B**) Comparison of XRD patterns for the rejuvenated and 17.7-year-aged $Ce_{70}Al_{10}Cu_{20}$ MGs. The inset displays the appearance of a 17.7-year-aged sample with a diameter of 2 mm. a.u., arbitrary units. (**C**) A high-resolution TEM micrograph of the hyperaged sample. The inset shows the diffractive halo-like selected-area electron diffraction, indicating the fully glassy state after prolonged aging.

Inset in Fig. 1B displays the appearance of a hyperaged sample with a light blue oxide layer on its surface. When the oxide layer is removed by sandpaper, the surface is as bright as that of the as-cast one (*18*). Typical high-resolution electron microscopy image and the corresponding selected area electron diffraction pattern shown in Fig. 1C further confirm its glassy nature without nanocrystals.

Kinetic and thermodynamic stability

Heat capacity curves for the fully rejuvenated and 1-, 10-, 49-, 79-, 325-, 1043-, 4597-, 5215-, and 6443-day-aged $Ce_{70}Al_{10}Cu_{20}$ MGs are given in Fig. 2A, which mainly focus on the glass transition region. It is found that the heat capacity curves of the rejuvenated and 1-day-aged samples are nearly the same. To further check the short-time aging effect, the heat capacity curve of a 300-s-aged sample is also measured and presented in fig. S1 for a clear display. It is shown that the heat capacity curve of the 300-s-aged sample is almost identical to those of the rejuvenated and 1-day-aged samples. For the 10-day-aged sample, its heat capacity curve in the glass transition region starts to change compared with that of the 1-day-aged sample, and a more pronounced endothermic peak is observed. These results suggest that within the short aging time of around 1 day, the relaxation process of the present sample is still not substantially activated by RT aging. While the aging time increases to more than 1 day, the onset temperature of glass transition in the heating process rises gradually, and the endothermic peaks during the glass transition become more and more pronounced. A distinct increase of onset temperature $\Delta T \sim 27$ K between the rejuvenated and 6443-day-aged samples could be observed in Fig. 2A, suggesting a significantly enhanced kinetic stability. In addition, there are no perceptible distinctions of crystallization temperature (T_x) and crystallization enthalpy (ΔH_x) of these samples for different aged states (see fig. S1), ruling out the possibility of nanocrystal precipitation during the prolonged aging process.

To further quantify the thermodynamic stability of the hyperaged $Ce_{70}Al_{10}Cu_{20}$ MG, T_g from the cooling process and the fictive temperature (T_f) have been determined. T_g is theoretically regarded as a measure of the temperature range where vitrification occurs on cooling from the liquid state, and it is defined as the intersection of the extrapolated glass and liquid line made on cooling (*19*). However, because of the supercooling issue (crystallization under nonthermodynamic equilibrium conditions) in differential scanning calorimetry (DSC) measurements, it is difficult to obtain the correct T_g value from the cooling process. Simon and co-workers have shown that the value of T_g is approximately equal to that of T_f (*20*). Therefore, one can directly take T_f from heating as T_g on cooling (*20*). The concept of T_f was first introduced by Tool (*21*) and was defined as "the temperature at which the glass would find itself in equilibrium if suddenly brought to it from its given state." It is an important parameter to describe thermal history and a measure of the average level of its corresponding liquid on the PEL. Here, T_f is obtained from the intersection between the extrapolated glass and liquid lines shown in Fig. 2B, and its accuracy has been confirmed by Moynihan area matching method (see the Supplementary Materials). As the value of T_g is almost the same as that of T_f, the aging time–dependent T_g for $Ce_{70}Al_{10}Cu_{20}$ MGs is obtained (fig. S2). It is found that T_g has no change in the initial aging time below about 1 day, then starts to decrease, and lastly approaches the aging temperature T_a with increasing aging time. Obviously, the 6443-day-aged $Ce_{70}Al_{10}Cu_{20}$ MG has a much lower T_g ($\Delta T_g \sim 46$ K) than those of its rejuvenated sample, demonstrating the higher thermodynamic stability.

Figure 2C shows the aging time t_a–dependent recovered enthalpy $\Delta H_{rec}(T_a, t_a)$. When t_a extends to infinity, it can be expected that ΔH_{rec} will reach a saturation value; eventually, the sample stays at an equilibrium glassy state, and the density of flow units (FU) would be exhausted (*22*). The exhaustion process of FU can be approached as $1/t_a$ term, and then, the recovered enthalpy can be well depicted as $\Delta H_{rec}(T_a, t_a) = \Delta H_{eq}/[1 + (\tau/t_a)^{\beta}]$, where ΔH_{eq} is the saturation value at $t_a \to \infty$, τ is the characteristic relaxation time, and β is a fitting parameter. Considering that the aging process has not been activated initially in the short-time region below about 1 day, only the recovery

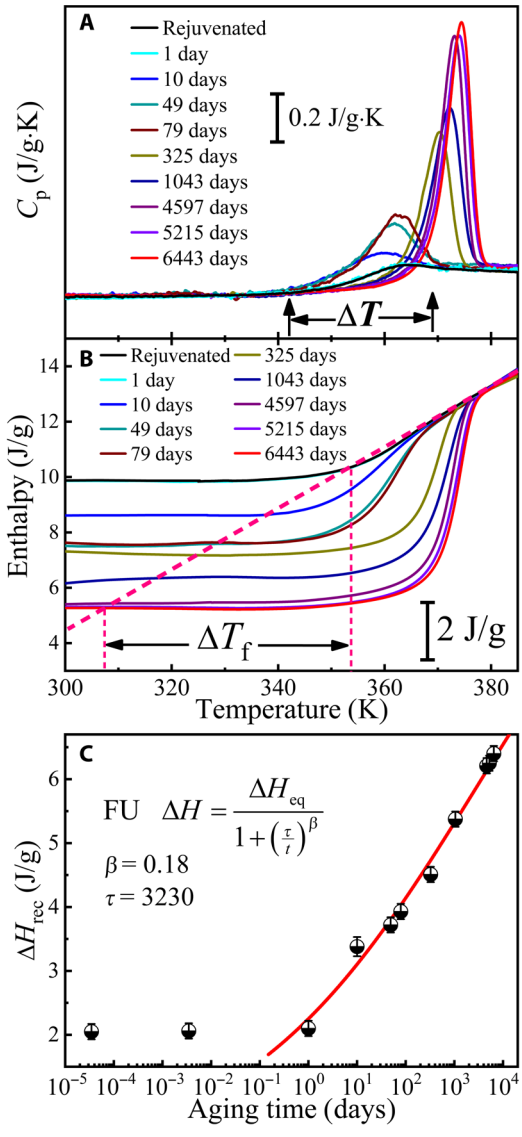

Fig. 2. Thermodynamic evolution behavior of $Ce_{70}Al_{10}Cu_{20}$ MGs with different aged states. (**A**) Heat capacity C_p of the rejuvenated and the aged $Ce_{70}Al_{10}Cu_{20}$ MGs for 1, 10, 49, 79, 325, 1043, 4597, 5215, and 6443 days, respectively, at RT. (**B**) Enthalpy curves are obtained by integrating the heat capacity shown in (A). Schematic plot for the definition of T_f: the intersection between extrapolated enthalpy of the supercooled liquid and that of its corresponding glass. The accuracy of T_f has been checked by using Moynihan area matching method (fig. S3) (*46*). (**C**) The recovery enthalpy of the samples with aging times from 1 to 6443 days is fitted by an exponential function from flow unit (FU) model. The relaxation time of the rejuvenated sample is roughly estimated to be about 3 s from the reciprocal of its cooling rate of 20 K/min. The values of recovery enthalpy of the samples with the short aging times of 3 s (3.47×10^{-5} day) and 300 s (3.47×10^{-3} day) are also plotted, and they do not show any changes within measuring errors. Because the relaxation process due to aging has not been activated at the short aging time below about 1 day, only the enthalpy values of the aging times ranging from 1 to 6443 days were taken to be fitted by the relaxation model.

enthalpy of the samples with aging times ranging from 1 to 6443 days is used to be fitted by the FU model. Accordingly, τ and β are fitted to be 3230 days and 0.18, respectively. The value of β is similar to the result obtained by other model (fig. S4). We note that the low β value is due to the temperature effect (measured below T_g), and the β value increases as aging temperature approaches T_g (fig. S5). The β value was found to be correlated with the movement scale of FU (*23*). For the lower value of β in the present work, the activation of FU is isolated and lacks large-scale cooperative motion during annealing, which is crucial for preventing crystallization and maintaining the glassy state (*22*, *23*).

Densification is the expected consequence when a glass is aged below T_g, because aging leads to the annihilation of excess free volume and allows for more efficient atomic packing with higher density and modulus. The density ρ, Young's modulus E, and shear modulus G of the rejuvenated and 17.7-year-aged $Ce_{70}Al_{10}Cu_{20}$ MGs and the rejuvenated and 110-million-year-aged amber (*3*) are collected in table S4. The values of ρ, E, and G of the rejuvenated $Ce_{70}Al_{10}Cu_{20}$ MG are 6.702 g/cm^3, 29.93 GPa, and 11.26 GPa, respectively. After RT aging for 17.7 years, the ρ, E, and G values of $Ce_{70}Al_{10}Cu_{20}$ MG increase by 1.2, 4.3, and 4.3%, respectively. A similar situation holds for amber where ρ, E, and G values are 2.1, 7.3, and 7.0% greater, respectively, for the 110-million-year-aged sample as compared to the rejuvenated amber. The relative changes of ρ, E, and G values for the hyperaged $Ce_{70}Al_{10}Cu_{20}$ MG and amber are much higher than those induced by conventional short-time annealing on glasses (*24*), indicating that a prominent densification resulted from prolonged aging.

The enhanced kinetic and thermodynamic stability with higher onset temperature and lower T_f has also been observed in the hyperaged amber (*3*, *4*), polystyrene (PS) (*25*), and the vapor-deposited organic 1,3-bis-(1-naphthyl)-5-(2-naphthyl)benzene (TNB) (*11*), indomethacin (IMC) (*11*), PS (*26*), and Teflon (*13*, *27*). While only the kinetic stability is enhanced for the vapor-deposited ZrCuAl MG (*14*, *15*), their thermodynamic stability becomes worse. As listed in table S3, ΔT (~27 K) of the hyperaged $Ce_{70}Al_{10}Cu_{20}$ MG is comparable to that of ultrastable IMC (24 K) (*11*) and superior to the effects in Zr-Cu-Al (11 K) (*14*) and 110-million-year-old amber (15 K) (*3*). Higher kinetic stability of the hyperaged $Ce_{70}Al_{10}Cu_{20}$ is due to higher temperatures that are required to dislodge the atoms from the trapped glassy configuration into a mobile equilibrium supercooled liquid. The considerable reduction of T_f, $\Delta T_f \sim 46$ K, indicates that the hyperaged $Ce_{70}Al_{10}Cu_{20}$ has entered into a fairly deeper basin in PEL with respect to the rejuvenated state and is an amber-like MG with both super thermodynamic and kinetic stability. The evolution of T_f is capable of characterizing the trend of a glassy structure toward the ideal glassy state (*28*).

To quantify how far away the glassy system is from the ideal glass state in the PEL, a parameter θ ($= 1 - \theta_K = \frac{T_f - T_K}{T_g - T_K}$) proposed by Swallen *et al.* (*11*) was used, where T_K is the Kauzmann temperature. T_K is the temperature below which the extrapolated entropy of the supercooled liquid would be less than that of the corresponding crystal (*29*), which has been thought to be representative of the ideal glass. As shown in Fig. 3, glassy materials can gradually approach the ideal glassy state by vapor deposition or conventional aging method. The θ values for the vapor-deposited IMC (*11*), TNB (*11*), and toluene (TL) (*30*) glasses are about 0.5, and Yoon *et al.* (*13*, *27*) reported a kind of vapor-deposited Teflon glass that reaches an extremely low θ value of 0.0385. The T_K value of $Ce_{70}Al_{10}Cu_{20}$ MG is estimated to be 290.8 K (fig. S6). The θ value of $Ce_{70}Al_{10}Cu_{20}$ MG is gradually reduced to 0.29 during the long-term aging, demonstrating that it has proceeded 71% toward the

ideal glass state in the PEL. In contrast, after conventional aging at $0.95T_g$ for about 1 year, the θ values for IMC (*28*) and PS (*25*) polymer glasses eventually decrease to 0.79 and 0.89, respectively, and the decrease rates of θ upon aging time for the polymer glasses are much smaller than that of $Ce_{70}Al_{10}Cu_{20}$ MG. The 20-million-year-old amber (*4*) exhibits a θ value of 0.39 that is slightly higher than that of the hyperaged CeAlCu MG. The short-time annealing can also enhance the thermodynamic and kinetic stability of MGs (*8*, *31*, *32*). For example, the $Au_{49}Cu_{26.9}Ag_{5.5}Pd_{2.3}Si_{16.3}$ MG annealed at $0.89T_g$ for 1×10^5 s can increase onset temperature by about 28 K with an enthalpy decrease of about 8.7 J/g (*31*), and 1 week of annealing at $0.94T_g$ can increase onset temperature by about 13 K with an enthalpy decrease of about 5.5 J/g for $Pd_{42.5}Cu_{30}Ni_{7.5}P_{20}$ (*32*). However, the θ values for $Au_{49}Cu_{26.9}Ag_{5.5}Pd_{2.3}Si_{16.3}$ (*31*) and $Pd_{42.5}Cu_{30}Ni_{7.5}P_{20}$ (*32*) are estimated to be 0.44 and 0.53, respectively, which are much higher than 0.32 of the hyperaged $Ce_{70}Al_{10}Cu_{20}$. Among MGs, which have poor glass-forming ability and stability among glassy materials, our aged Ce-based bulk MG is, so far, closest to the bottom of the PEL and superstable.

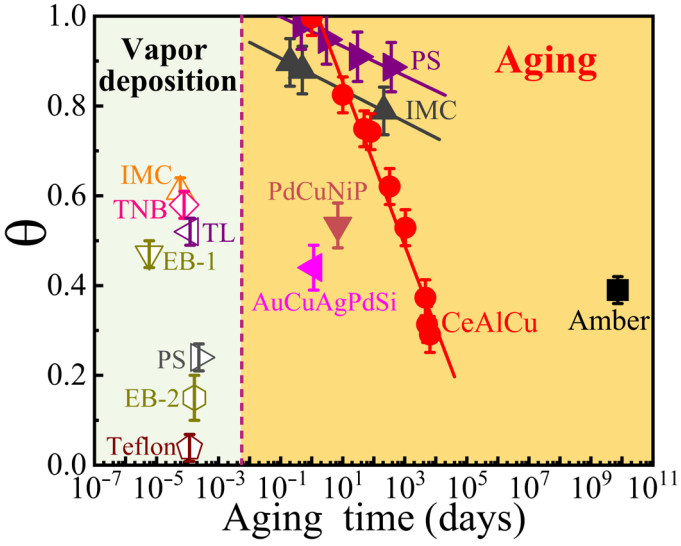

Fig. 3. The parameter $\theta = (T_f - T_K)/(T_g - T_K)$ was used to describe how far away the glassy system is from the ideal glass state in the PEL. Aging time log*t* versus θ for the vapor-deposited IMC (*11*), TNB (*11*), TL (*30*), ethylbenzene (EB) (*47*, *48*), PS (*26*), and Teflon (*13*, *27*) and conventionally aged $Ce_{70}Al_{10}Cu_{20}$, $Au_{49}Cu_{26.9}Ag_{5.5}Pd_{2.3}Si_{16.3}$ (*31*), $Pd_{42.5}Cu_{30}Ni_{7.5}P_{20}$ (*32*), amber (*3*), IMC (*28*), and PS (*25*). Solid line is the best fitting result through a linear function for PS, IMC, and CeAlCu. The aging time for the vapor-deposited samples was estimated by the time taken to prepare a film of 1 nm in thickness.

DISCUSSION

It is known that the metastable MGs cannot be annealed for a long time near T_g; otherwise, it would precipitate nanocrystals and gradually crystallize (*2*, *6*). As shown in Fig. 4, MGs usually have poor resistance against crystallization at high temperature around T_g, and short-time annealing near T_g of Zr-, Cu-, Pd-, and Al-based MGs easily leads to the precipitation of nanocrystals and crystallization. On the other hand, for long-term aging on MGs, such as CuZr MG aged for years at RT (about $0.44T_g$) far below T_g, the micron-scale Cu crystal precipitates, showing poor ability against crystallization (*10*). However, the present $Ce_{70}Al_{10}Cu_{20}$ MG maintains a fully amorphous state after aging at relatively high temperature (~$0.85T_g$) for more than 17 years, showing an extremely strong resistance against crystallization. The hyperaged Ce-based MG not only is in a thermodynamic low energy state in the PEL but also has an exceptionally strong resistance against crystallization, which makes it similar to amber (see Fig. 4) (*3*, *4*). To our knowledge, such an amber-like

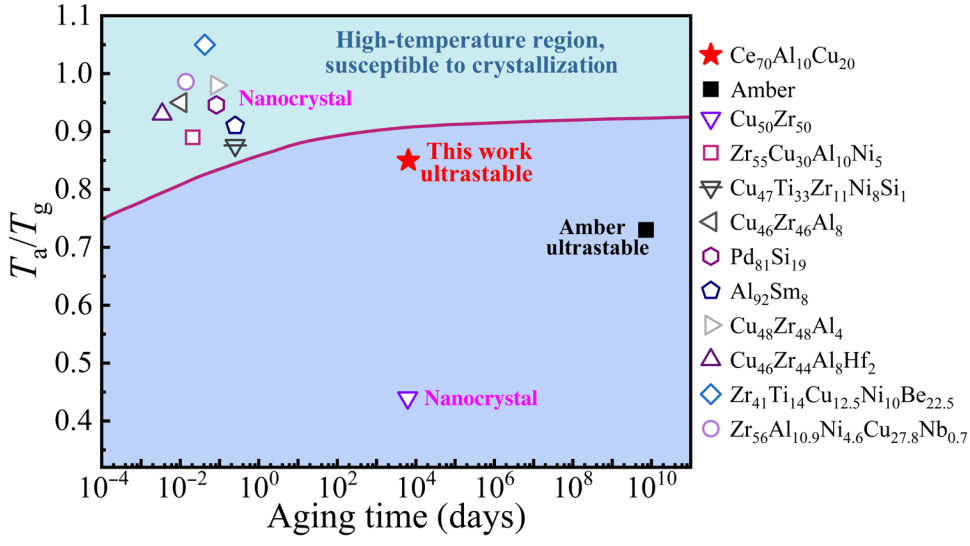

Fig. 4. The resistance against crystallization for MGs and amber when they are annealed at different temperature ranges for different periods of time. When the Zr-, Cu-, Pd-, and Al-based MGs are annealed near T_g for a short time (T_a is annealing temperature), nanocrystals are likely to precipitate and gradually crystallize. The $Cu_{50}Zr_{50}$ MG crystallized after aging at RT (about $0.44T_g$) for years (*10*). The 20-million-year-old amber shows super thermal stability against crystallization (*4*). The present CeAlCu MG maintains a fully amorphous state even after RT (about $0.85T_g$) aging for more than 17 years and exhibits a kind of amber-like stability. For the specific data, refer to table S5.

strong resistance against crystallization has never been reported in known MGs.

Another issue of current interest is why $Ce_{70}Al_{10}Cu_{20}$ MG can achieve a deeper basin than most glassy materials under aging and how it accomplishes this process. It is known that glasses can be classified as either strong or fragile liquids according to the extent of viscosity that deviates from Arrhenius behavior around T_g. In general, strong glasses have almost constant activation energy to relaxation and display strong landscapes consisting of a single megabasin, whereas fragile glasses exhibit variable activation energy and a diversity of well-separated megabasins (*33*, *34*). The fragility of $Ce_{70}Al_{10}Cu_{20}$ MG was measured to be ~28 (*17*), which is much stronger than that of organic IMC [~82.8 (*16*)] and PS [~116 (*16*)]. Although IMC (*28*) and PS (*25*) were aged at higher temperature around $0.95T_g$, the decline rates of θ along the aging time for fragile IMC and PS are much smaller than that of strong $Ce_{70}Al_{10}Cu_{20}$ MG (see Fig. 3). The relaxation rate of a glass can also be simply evaluated by its activation energy (*35*). According to the heating rate–dependent T_g shown in fig. S7, the activation energy of $Ce_{70}Al_{10}Cu_{20}$ MG is calculated to be 210.8 kJ/mol. The T_g values of PS (373 K) and IMC (314 K) are similar to that of $Ce_{70}Al_{10}Cu_{20}$ MG. However, the activation energies of PS and IMC were measured to be 774 and 340 kJ/mol (*36*, *37*), respectively, which are much higher than that of $Ce_{70}Al_{10}Cu_{20}$ MG. Thus, the relaxation rate of $Ce_{70}Al_{10}Cu_{20}$ MG is expected to be higher than those of PS and IMC. The above scenario can be understood by the schematic diagram in Fig. 5. Upon aging or deposition, fragile glass is easily trapped in a megabasin with local minimum energy. Conversely, the structural relaxation for strong glass can be realized by continuous basin hopping until it infinitely approaches the ideal glass state. Thus, strong glass is able to keep going down to a lower energy state as long as there is sufficient aging time. The small value of $m \sim 28$ demonstrates that Ce-based liquids belong to the strong glass formers, and the structural origin of strong liquid behavior is closely related to the existence of partial covalent bonding formed by Ce-4*f* electron delocalization (*38*). The higher the interaction potential among the particles constituting the system, the stronger is the fragility (*39*). The strong covalent bonding in Ce-based MG makes it one of the strongest glass formers.

As discussed above, the strong fragility provides chances for MGs to be annealed effectively toward the ideal state. However, the crystal nucleation still could intervene the long-term aging and transform the glass to crystal. We then also consider the resistance against crystallization of the Ce-based MG. We estimate the homogeneous nucleation frequency I based on the classical nucleation theory (*40*, *41*) and the relation between viscosity and fragility (*42*). The resulted homogeneous nucleation frequency I can be expressed as

$$I = k_n / \left(\eta_0 \exp\left(\frac{2\ln 10\, {m_{\min}}^2 T_{rg}}{(3T_r - 2T_{rg})(m - m_{\min})} \right) \right) \exp\left(\frac{-b(\alpha\beta^{1/3})^3}{T_r (1 - T_r)^2} \right) \quad (1)$$

where k_n, b, and η_0 are constants; α and β are dimensionless parameters; $T_r = T/T_l$ is reduced temperature; and $m_{\min}$ is the minimum value of fragility. Therefore, I can be described as a function of fragility m and T_{rg} parameter, and the detailed calculation procedure of I is given in the Supplementary Materials. Figure 6 shows the nucleation frequency differences between CeAlCu and other MGs with poor stability as seen in Fig. 4. It is obvious that the nucleation frequency of CeAlCu over a wide range of temperature is much lower than that of other MGs with poor stability, demonstrating the excellent stability of CeAlCu MG against nucleation. According to Eq. 1, the variation of nucleation frequency I is mainly determined by fragility m and T_{rg} parameter. We have further analyzed the contribution of m and T_{rg} to nucleation frequency I in the Supplementary

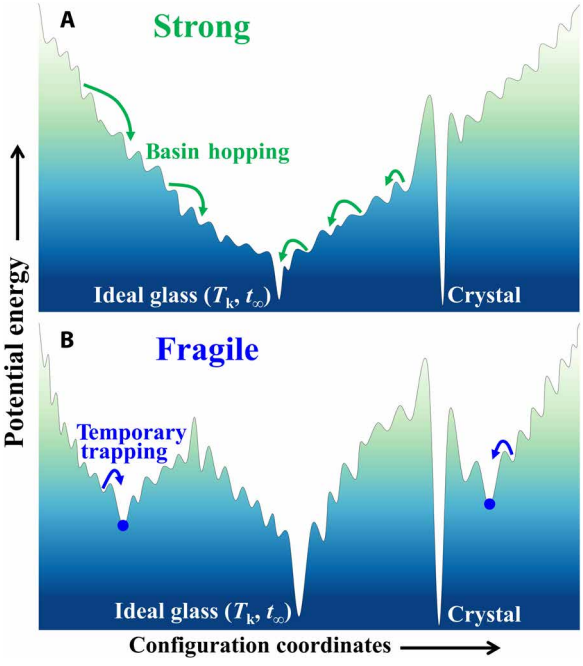

Fig. 5. Schematic diagram of the PEL for strong and fragile glassy system. (**A**) Strong glass with a single megabasin can relax to approach the ideal glass by continuous basin hopping. (**B**) Fragile glass with diverse megabasins is easily trapped in a local megabasin.

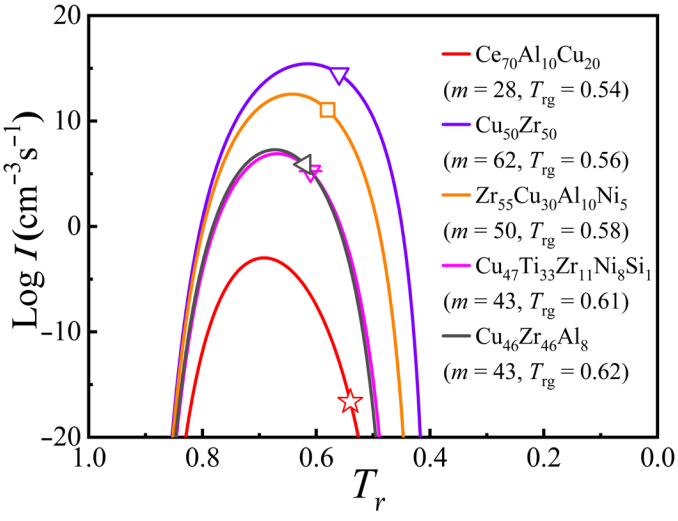

Fig. 6. Homogeneous nucleation frequency was calculated to evaluate the resistance of MGs to nucleation. Reduced temperature ($T_r = T/T_l$)–dependent logarithm of homogeneous nucleation frequency of CeAlCu and other MGs with poor stability shown in Fig. 4. The open symbols represent the values of nucleation frequency at T_g point.

Materials, and we show that m plays a dominant role in determining I compared to T_{rg}, especially when m is less than 35. Therefore, the low nucleation frequency of CeAlCu MG benefits mainly from its extremely strong fragility, whose structural origin is closely related to the existence of partial covalent bonding formed by Ce-4*f* electron delocalization (*38*).

Few experiments in polymer and selenium glasses (*43*, *44*) have found that nucleation occurs only after the completion of the enthalpy relaxation. However, it is controversial whether the metastable solid MGs can reach equilibrium liquid state before nucleation, because the enthalpy reduction of MG is usually so small in the short-time annealing process that it is hard to measure using a conventional DSC. The present CeAlCu MG with long-aging history is suitable for studying this controversy through the signatures of the glassy kinetics developed by Kovacs (*45*). The first one is the isothermal aging of CeAlCu MG at RT below T_g for a long enough time. As presented in Fig. 7A, if CeAlCu MG ages for a long enough time, then it can eventually reach equilibrium liquid state (yellow solid dot), where T_f is equal to aging temperature T_a. The current 17.7-year aging has driven the rejuvenated sample to a very deep position (green solid dot), which is close to the equilibrium liquid state but not yet reached. The heat capacity curves in fig. S1 show that the exothermic crystallization enthalpy and onset temperature of crystallization are almost invariable with the aging time, demonstrating that there is no crystal growing into nanocrystals during the aging process toward equilibrium liquid state.

It has been reported that the glassy kinetics can also be observed by the asymmetrical approaching experiment developed by Kovacs (*45*). It is expected that the asymmetrical approaching experiment (partial aging at a low temperature and jumping to a higher temperature) can result in a crossover event where the enthalpy of the sample first rises across that of the equilibrium liquid and then falls back to that of the equilibrium liquid state due to the memory effect. Thus, an endothermic peak of enthalpy recovery followed by an exothermic peak of overshoot could be observed from the corresponding time-dependent heat flow curve. As presented in Fig. 7A, the enthalpy differences between the 6443-day-old sample and its equilibrium liquid at 348 and 353 K are 4.39 and 4.85 J/g, respectively. Here, the enthalpy curves of the rejuvenated and 6443-day-old CeAlCu MGs are taken from Fig. 2B. The 6443-day-old CeAlCu MG was heated rapidly from RT to higher temperatures of 348 and 353 K and then kept their isothermal states, as indicated by the violet and magenta dotted lines in Fig. 7A, respectively. As shown in Fig. 7B, endothermic peaks with enthalpy of 4.65 and 5.13 J/g are observed for the isothermal annealing at 348 and 353 K, respectively. These values are obviously higher than the above enthalpy differences between the 6443-day-old sample and its equilibrium liquid, indicating that the enthalpy of the sample has already crossed above that of the equilibrium liquid during the asymmetrical approaching experiments. Unfortunately, we did not observe an exothermic peak representing a decrease in enthalpy as it retreats toward the equilibrium liquid. This is probably because the overshoot enthalpy is so small that it is difficult to observe the exothermic peak by a traditional DSC instrument.

The above asymmetrical approaching experiments have demonstrated that the hyperaged CeAlCu sample has reached the equilibrium liquid state during the asymmetrical approaching experiments at temperatures of 348 and 353 K. In fig. S9, we checked their DSC curves after the annealing experiments and found that their crystallization temperature and enthalpy of crystallization had almost no change compared with the rejuvenated and hyperaged samples. Therefore, for the present CeAlCu MG, we have confirmed that no crystallization occurs during the aging process to equilibrium liquid state, which is consistent with the idea that nucleation only occurs after the completion of enthalpy relaxation.

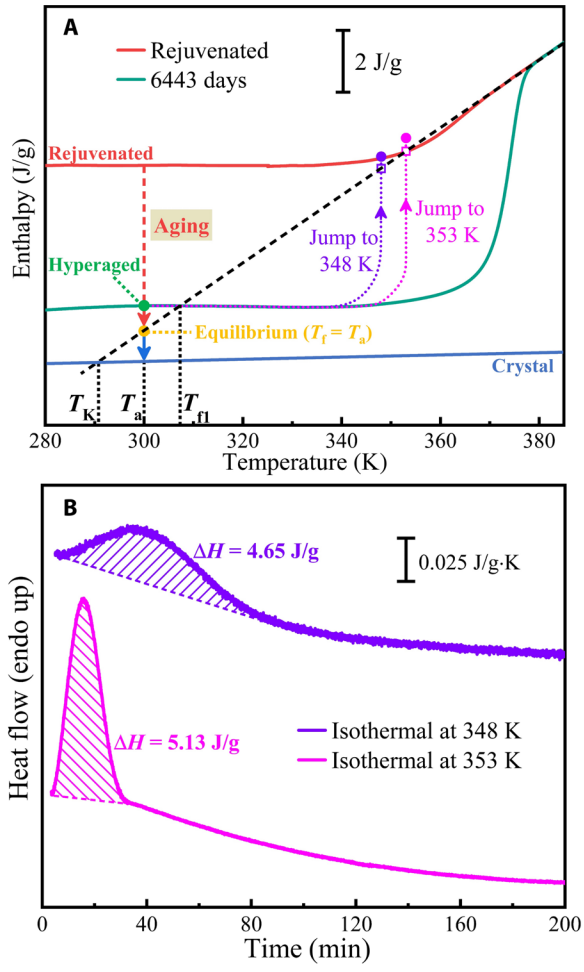

Fig. 7. The hyperaged CeAlCu sample can reach the equilibrium liquid state by asymmetrical approaching experiment. (**A**) Schematic diagram showing the enthalpy change during isothermal aging and asymmetrical approaching experiments. The black dotted line represents the extrapolated line of the supercooled liquid. The intersections between extrapolated enthalpy of the supercooled liquid and that of the corresponding glass and crystal are fictive temperature (T_{f1}) and Kauzmann temperature (T_k), respectively. As indicated by the red dashed line, the enthalpy of the rejuvenated sample has dropped to the position of the green dot after aging at T_a for 6443 days. If aging time is given long enough, then the enthalpy will eventually drop to the equilibrium position (yellow dot), where fictive temperature T_f is equal to aging temperature T_a. The violet and magenta dotted lines represent the enthalpy changes during the asymmetrical approaching experiment with rapid heating from RT to 348 and 353 K, respectively. The violet and magenta solid dots represent the positions to which the highest enthalpy reaches for the 6443-day-old sample in the asymmetrical approaching experiment with rapid heating from RT to 348 and 353 K, respectively. The violet and magenta empty squares represent the enthalpy of the equilibrium liquid at 348 and 353 K, respectively. (**B**) Time-dependent heat flow after the quick temperature jumps from RT to 348 and 353 K, respectively. The shaded area represents the enthalpy released during the isothermal process.

In summary, we show the $Ce_{70}Al_{10}Cu_{20}$ MG can reach ultrastable state by aging around its glass transition temperature even for more than 17 years, which is similar to amber. The obtained hyperstable MG state has highly kinetic stability to resist crystallization and exceptional thermodynamic stability that tend toward the ideal glass state. The hyperaged CeAlCu MG can reach the equilibrium liquid state without crystallization. The ultrastability is attributed to its relatively simple energy landscape and strong resistance against nucleation.

MATERIALS AND METHODS

MG preparation

Master alloy ingots with nominal atomic percent composition of $Ce_{70}Al_{10}Cu_{20}$ was prepared by arc melting of the individual elemental components (Ce: 99.5 weight %; Al: 99.99%; and Cu: 99.99%) in a Ti-gettered ultrahigh-purity Ar atmosphere. The ingot was remelted for more than four times and suction-cast into a Cu mold to prepare bulk glassy rods of 2 mm in diameter.

Aging and rejuvenation processes

As-cast $Ce_{70}Al_{10}Cu_{20}$ MG was produced in 2004 (*18*) and stored in a zipped plastic box under ambient condition for 12.6 years (4597 days), 14.3 years (5215 days), and 17.7 years (6443 days), respectively, to reach a hyperaged state. For comparison, rejuvenated $Ce_{70}Al_{10}Cu_{20}$ MG was obtained by heating the hyperaged sample to the temperature higher than the end of glass transition temperature by 5 K at 20 K/min, holding for 60 s, and then cooling down to RT at 20 K/min under a purified nitrogen atmosphere, thus erasing the thermal history of the hyperaged sample. Rejuvenated samples were naturally aged at RT for 300 s and 1, 10, 49, 79, 325, and 1043 days, respectively.

Amorphous structure characterization

The amorphous structure of hyperaged and rejuvenated samples was confirmed by a D/MAX2500V x-ray diffractometer using 40 kV, Cu Kα radiation (λ = 1.5405 Å) at a scanning rate of 4°/min, and in the range of 10° to 90° (2θ). Specimens for transmission electron microscopy (TEM) characterization were carefully prepared by ion milling with 3-keV Ar ions at the liquid nitrogen temperature. The high-resolution TEM images were captured using a JEM-2100F instrument operated at 200 kV.

DSC measurements

The PerkinElmer DSC 8000 was used to perform and examine the kinetics and thermodynamics of the samples at a heating rate of 10 K/min under flowing pure argon gas at 20 ml/min to prevent possible surface oxidation. To ensure the reliability of the data, temperature and enthalpy were calibrated with an indium and a zinc standard specimen, giving an accuracy of ±0.2 K and ±0.02 mW, respectively. Heat capacity (C_p) of $Ce_{70}Al_{10}Cu_{20}$ MGs was obtained by comparing with that of a sapphire standard sample. Identical measurement procedures were performed on the empty pan as a baseline to be subtracted from the sample and the sapphire. The specific heat capacity of the sample can be determined by

$$C_p(T)_{sample} = \frac{Q_{sample} - Q_{pan}}{Q_{sapphire} - Q_{pan}} \cdot \frac{m_{sapphire}}{m_{sample}} \cdot C_p(T)_{sapphire} \quad (2)$$

where m_i is the mass of sample and sapphire; Q_i is the heat flow of the empty pan, sample, and sapphire; and $C_p(T)_{sapphire}$ is the heat capacity of the standard sapphire. The asymmetrical approaching experiment was performed by quickly heating the hyperaged samples from RT at 100 K/min to 348 and 353 K and then keeping the temperature there for more than 10 hours.

Physical property measurements

The density ρ was determined using Archimedes' principle in distilled water, and the measuring uncertainties are within 0.2%. The acoustic longitudinal (v_l) and transverse (v_s) velocities of the rejuvenated and hyperaged CeAlCu MGs were measured at RT using a pulse echo overlap method (*24*). The travel time of ultrasonic waves propagating through the sample was measured using a MATEC 6600 ultrasonic system with a measuring sensitivity of 0.5 ns. The carrying frequency of the ultrasonic is 10 MHz. The Young's modulus E, shear modulus G, bulk modulus K, and Poisson's ratio σ were derived from the acoustic velocities and density as follows: $G = \rho v_s^2$; $K = \rho(v_l^2 - 4/3v_s^2)$; $\sigma = \rho(v_l^2 - 2v_s^2)/2(v_l^2 - v_s^2)$; $E = 2G(1 + \sigma)$.

SUPPLEMENTARY MATERIALS

Supplementary material for this article is available at https://science.org/doi/10.1126/sciadv.abn3623

REFERENCES AND NOTES

1. I. M. Hodge, Physical aging in polymer glasses. *Science* **267**, 1945–1947 (1995).
2. W. H. Wang, R. J. Wang, W. T. Yang, B. C. Wei, P. Wen, D. Q. Zhao, M. X. Pan, Stability of ZrTiCuNiBe bulk metallic glass upon isothermal annealing near the glass transition temperature. *J. Mater. Res.* **17**, 1385–1389 (2002).
3. T. Pérez-Castañeda, R. J. Jiménez-Riobóo, M. A. Ramos, Two-level systems and boson peak remain stable in 110-million-year-old amber glass. *Phys. Rev. Lett.* **112**, 165901 (2014).
4. J. Zhao, S. L. Simon, G. B. McKenna, Using 20-million-year-old amber to test the super-Arrhenius behaviour of glass-forming systems. *Nat. Commun.* **4**, 1783 (2013).
5. A. E. Saal, E. H. Hauri, M. L. Cascio, J. A. Van Orman, M. C. Rutherford, R. F. Cooper, Volatile content of lunar volcanic glasses and the presence of water in the Moon's interior. *Nature* **454**, 192–195 (2008).
6. W. Klement, R. H. Willens, P. Duwez, Non-crystalline structure in solidified gold-silicon alloys. *Nature* **187**, 869–870 (1960).
7. A. Castellero, B. Moser, D. I. Uhlenhaut, F. H. Dalla Torre, J. F. Löffler, Room-temperature creep and structural relaxation of Mg–Cu–Y metallic glasses. *Acta Mater.* **56**, 3777–3785 (2008).
8. O. Haruyama, Y. Nakayama, R. Wada, H. Tokunaga, J. Okada, T. Ishikawa, Y. Yokoyama, Volume and enthalpy relaxation in $Zr_{55}Cu_{30}Ni_5Al_{10}$ bulk metallic glass. *Acta Mater.* **58**, 1829–1836 (2010).
9. P. Xue, Y. J. Huang, S. Pauly, S. S. Jiang, S. Guo, Z. L. Ning, J. F. Sun, Long-term room-temperature aging treatment of a bulk metallic glass composite. *J. Alloy. Compd.* **820**, 153165 (2020).
10. D. V. Louzguine-Luzgin, J. Jiang, On long-term stability of metallic glasses. *Metals* **9**, 1076 (2019).
11. S. F. Swallen, K. L. Kearns, M. K. Mapes, Y. S. Kim, R. J. McMahon, M. D. Ediger, T. Wu, L. Yu, S. Satija, Organic glasses with exceptional thermodynamic and kinetic stability. *Science* **315**, 353–356 (2007).
12. Y. L. Guo, A. Morozov, D. Schneider, J. W. Chung, C. Zhang, M. Waldmann, N. Yao, G. Fytas, C. B. Arnold, R. D. Priestley, Ultrastable nanostructured polymer glasses. *Nat. Mater.* **11**, 337–343 (2012).
13. H. Yoon, G. B. McKenna, Testing the paradigm of an ideal glass transition: Dynamics of an ultrastable polymeric glass. *Sci. Adv.* **4**, eaau5423 (2018).
14. H.-B. Yu, Y. Luo, K. Samwer, Ultrastable metallic glass. *Adv. Mater.* **25**, 5904–5908 (2013).
15. P. Luo, C. R. Cao, F. Zhu, Y. M. Lv, Y. H. Liu, P. Wen, H. Y. Bai, G. Vaughan, M. Di Michiel, B. Ruta, W. H. Wang, Ultrastable metallic glasses formed on cold substrates. *Nat. Commun.* **9**, 1389 (2018).
16. C. P. Royall, F. Turci, S. Tatsumi, J. Russo, J. Robinson, The race to the bottom: Approaching the ideal glass? *J. Phys. Condens. Matter* **30**, 363001 (2018).
17. Y. Zhao, B. Zhang, Evaluating the correlation between liquid fragility and glass-forming ability in the extremely strong Ce-based bulk metallic glasses. *J. Appl. Phys.* **122**, 115107 (2017).

18. B. Zhang, D. Q. Zhao, M. X. Pan, W. H. Wang, A. L. Greer, Amorphous metallic plastic. *Phys. Rev. Lett.* **94**, 205502 (2005).
19. G. B. McKenna, S. L. Simon, The glass transition: Its measurement and underlying physics, in *Handbook of Thermal Analysis and Calorimetry* (Elsevier, 2002).
20. P. Badrinarayanan, W. Zheng, Q. X. Li, S. L. Simon, The glass transition temperature versus the fictive temperature. *J. Non Cryst. Solids* **353**, 2603–2612 (2007).
21. A. Q. Tool, Relaxation between inelastic deformability and thermal expansion of glass in its annealing range. *J. Am. Ceram. Soc.* **29**, 240–253 (1964).
22. Z. Lu, W. Jiao, W. H. Wang, H. Y. Bai, Flow unit perspective on room temperature homogeneous plastic deformation in metallic glasses. *Phys. Rev. Lett.* **113**, 045501 (2014).
23. Z. Wang, B. A. Sun, H. Y. Bai, W. H. Wang, Evolution of hidden localized flow during glass-to-liquid transition in metallic glass. *Nat. Commun.* **5**, 5823 (2014).
24. W. H. Wang, The elastic properties, elastic models and elastic perspectives of metallic glasses. *Prog. Mater. Sci.* **57**, 487–656 (2012).
25. Y. P. Koh, S. L. Simon, Enthalpy recovery of polystyrene: Does a long-term aging plateau exist? *Macromolecules* **46**, 5815–5821 (2013).
26. A. N. Raegen, J. J. Yin, Q. Zhou, J. A. Forrest, Ultrastable monodisperse polymer glass formed by physical vapour deposition. *Nat. Mater.* **19**, 1110–1113 (2020).
27. H. Yoon, Y. P. Koh, S. L. Simon, G. B. McKenna, An ultrastable polymeric glass: Amorphous fluoropolymer with extreme fictive temperature reduction by vacuum pyrolysis. *Macromolecules* **50**, 4562–4574 (2017).
28. K. L. Kearns, S. F. Swallen, M. D. Ediger, T. Wu, Y. Sun, L. Yu, Hiking down the energy landscape: Progress toward the Kauzmann temperature via vapor deposition. *J. Phys. Chem. B* **112**, 4934–4942 (2008).
29. W. Kauzmann, The nature of the glassy state and the behavior of liquids at low temperatures. *Chem. Rev.* **43**, 219–256 (1948).
30. A. Sepúlveda, E. Leon-Gutierrez, M. Gonzalez-Silveira, C. Rodríguez-Tinoco, M. T. Clavaguera-Mora, J. Rodriguez-Viejo, Accelerated aging in ultrathin films of a molecular glass former. *Phys. Rev. Lett.* **107**, 025901 (2011).
31. J. Q. Wang, Y. Shen, J. H. Perepezko, M. D. Ediger, Increasing the kinetic stability of bulk metallic glasses. *Acta Mater.* **104**, 25–32 (2016).
32. O. Haruyama, T. Mottate, K. Morita, N. Yamamoto, H. Kato, T. Egami, Volume and enthalpy relaxation in $Pd_{42.5}Cu_{30}Ni_{7.5}P_{20}$ bulk metallic glass. *Mater. Trans.* **55**, 466–472 (2014).
33. L.-M. Martinez, C. A. Angell, A thermodynamic connection to the fragility of glass-forming liquids. *Nature* **410**, 663–667 (2001).
34. P. G. Debenedetti, F. H. Stillinger, Supercooled liquids and the glass transition. *Nature* **410**, 259–267 (2001).
35. L. Boehm, M. D. Ingram, C. A. Angell, Test of a year-annealed glass for the cohen-grest percolation transition. *J. Non Cryst. Solids* **44**, 305–313 (1981).
36. R. M. Kimmel, D. R. Uhlmann, Activation energy spectra for relaxation in amorphous materials. I. Volume relaxation in polystyrene and polyvinyl acetate. *J. Appl. Phys.* **40**, 4254–4260 (1969).
37. J. J. M. Ramos, R. Taveira-Marques, H. P. Diogo, Estimation of the fragility index of indomethacin by DSC using the heating and cooling rate dependency of the glass transition. *J. Pharm. Sci.* **93**, 1503–1507 (2004).
38. Y. Zhao, D. D. Li, B. Y. Qu, R. L. Zhou, B. Zhang, K. Sato, Anomalous packing state in Ce-Ga-Cu bulk metallic glasses. *Intermetallics* **84**, 25–29 (2017).
39. T. Scopigno, G. Ruocco, F. Sette, G. Monaco, Is the fragility of a liquid embedded in the properties of its glass? *Science* **302**, 849–852 (2003).
40. D. Turnbull, Under what conditions can a glass be formed? *Contemp. Phys.* **10**, 473–488 (1969).
41. J. H. Hollomon, D. Turnbull, Nucleation. *Prog. Met. Phys.* **4**, 333–388 (1953).
42. C. A. Angell, K. L. Ngai, G. B. McKenna, P. F. McMillan, S. W. Martin, Relaxation in glassforming liquids and amorphous solids. *J. Appl. Phys.* **88**, 3113–3157 (2000).
43. R. Androsch, C. Schick, J. W. P. Schmelzer, Sequence of enthalpy relaxation, homogeneous crystal nucleation and crystal growth in glassy polyamide 6. *Eur. Polym. J.* **53**, 100–108 (2014).
44. I. Stolte, R. Androsch, M. L. Di Lorenzo, C. Schick, Effect of aging the glass of isotactic polybutene-1 on form II nucleation and cold crystallization. *J. Phys. Chem. B* **117**, 15196–15203 (2013).
45. A. J. Kovacs, Transition vitreuse dans les polymères amorphes. Etude phénomènologique, in *Fortschritte Der Hochpolymeren-Forschung. Advances in Polymer Science* (Springer, 1964), vol. 3/3, pp. 394–507.
46. C. T. Moynihan, A. J. Easteal, M. A. De Bolt, J. Tucker, Dependence of the fictive temperature of glass on cooling rate. *J. Am. Ceram. Soc.* **59**, 12–16 (1976).
47. S. L. L. M. Ramos, M. Oguni, K. Ishii, H. Nakayama, Character of devitrification, viewed from enthalpic paths, of the vapor-deposited ethylbenzene glasses. *J. Phys. Chem. B* **115**, 14327–14332 (2011).
48. M. S. Beasley, C. Bishop, B. J. Kasting, M. D. Ediger, Vapor-deposited ethylbenzene glasses approach "ideal glass" density. *J. Phys. Chem. Lett.* **10**, 4069–4075 (2019).
49. O. Kubaschewski, C. B. Alcock, P. J. Spencer, *Materials Thermo-Chemistry* (Pergamon, ed. 6, 1993).
50. T. Komatsu, Application of fragility concept to metallic glass formers. *J. Non Cryst. Solids* **185**, 199–202 (1995).
51. L. M. Wang, Y. J. Tian, R. P. Liu, W. H. Wang, A "universal" criterion for metallic glass formation. *Appl. Phys. Lett.* **100**, 261913 (2012).
52. Z. P. Lu, Y. Li, C. T. Liu, Glass-forming tendency of bulk La–Al–Ni–Cu–(Co) metallic glass-forming liquids. *J. Appl. Phys.* **93**, 286–290 (2002).
53. M. Lasocka, The effect of scanning rate on glass transition temperature of splat-cooled $Te_{85}Ge_{15}$. *Mater. Sci. Eng.* **23**, 173–177 (1976).
54. Z. L. Long, H. Q. Wei, Y. H. Ding, P. Zhang, G. Q. Xie, A. Inoue, A new criterion for predicting the glass-forming ability of bulk metallic glasses. *J. Alloys Compd.* **475**, 207–219 (2009).
55. Z. Chen, R. Richert, Dynamics of glass-forming liquids. XV. Dynamical features of molecular liquids that form ultra-stable glasses by vapor deposition. *J. Chem. Phys.* **135**, 124515 (2011).
56. S. Venkataraman, H. Hermann, D. J. Sordelet, J. Eckert, Influence of sub-T_g annealing on the crystallization kinetics of $Cu_{47}Ti_{33}Zr_{11}Ni_8Si_1$ metallic glass. *J. Appl. Phys.* **104**, 066107 (2008).
57. N. Van Steenberge, A. Concustell, J. Sort, J. Das, N. Mattern, A. Gebert, S. Suriñach, J. Eckert, M. Baró, Microstructural inhomogeneities introduced in a Zr-based bulk metallic glass upon low-temperature annealing. *Mater. Sci. Eng. A* **491**, 124–130 (2008).
58. J. H. Perepezko, R. J. Hebert, W. S. Tong, J. Hamann, H. R. Rösner, G. Wilde, Nanocrystallization reactions in amorphous aluminum alloys. *Mater. Trans.* **44**, 1982–1992 (2003).
59. B. Sarac, A. Bernasconi, J. Wright, M. Stoica, F. Spieckermann, M. Mühlbacher, J. Keckes, X. Bian, G. Wang, J. Eckert, Structural modifications in sub-T_g annealed CuZr-based metallic glass. *Mater. Sci. Eng. A* **707**, 245–252 (2017).
60. A. Rezvan, B. Sarac, V. Soprunyuk, J. T. Kim, K. K. Song, C. J. Li, W. Schranz, J. Eckert, Influence of combinatorial annealing and plastic deformation treatments on the intrinsic properties of $Cu_{46}Zr_{46}Al_8$ bulk metallic glass. *Intermetallics* **127**, 106986 (2020).
61. N. Chen, K.-F. Yao, F. Ruan, Microstructural features of phase transformation in a binary Pd–Si metallic glass. *Philos. Mag. Lett.* **87**, 677–686 (2007).
62. R. Wei, X. L. Wang, S. Yang, F. Jiang, L. He, Formation of CuZr-based bulk metallic glass composites containing nanometer-scale B2-CuZr phase through sub-T_g annealing. *J. Alloys Compd.* **617**, 699–706 (2014).
63. M. Song, X. Z. Liao, Y. H. He, Effect of sub-T_g annealing on the mechanical properties of a ZrAlNiCuNb bulk metallic glass. *Philos. Mag. Lett.* **91**, 713–723 (2011).
64. Y. X. Zhuang, W. H. Wang, Effects of relaxation on glass transition and crystallization of ZrTiCuNiBe bulk metallic glass. *J. Appl. Phys.* **87**, 8209–8211 (2000).

Acknowledgments

Funding: This work was financially supported by Guangdong Major Project of Basic and Applied Basic Research, China (grant no. 2019B030302010); the National Key Research and Development Program of China (grant no. 2021YFA0716302); the National Natural Science Foundation of China (grant nos. 52101199 and 52071222); the Program for the Experiments for Space Exploration from the Qian Xuesen Laboratory, China Academy of Space Technology (contract no. TKTSPY-2020-03-02); and the Guangdong Basic and Applied Basic Research Foundation, China (grant no. 2021B1515140005). **Author contributions:** B.Z., H.B., and W.-H.W. conceived the idea and designed the experiments. Y.Z. performed the experiments, analyzed the data, and wrote the manuscript. Y.Z., B.Z., B.S., X.T., H.K., H.B., and W.-H.W. discussed the data and wrote the manuscript. All authors participated in preparing the paper and the result discussions. **Competing interests:** The authors declare that they have no competing interests. **Data and materials availability:** All data needed to evaluate the conclusions in the paper are present in the paper and/or the Supplementary Materials.

Submitted 22 November 2021
Accepted 1 July 2022
Published 17 August 2022
10.1126/sciadv.abn3623

ScienceAdvances

Ultrastable metallic glass by room temperature aging

Yong ZhaoBaoshuang ShangBo ZhangXing TongHaibo KeHaiyang BaiWei-Hua Wang

Sci. Adv., 8 (33), eabn3623. • DOI: 10.1126/sciadv.abn3623

Science Advances (ISSN) is published by the American Association for the Advancement of Science. 1200 New York Avenue NW, Washington, DC 20005. The title *Science Advances* is a registered trademark of AAAS.